



**HAL**  
open science

# The polarity-induced force imbalance in *Caenorhabditis elegans* embryos is caused by asymmetric binding rates of dynein to the cortex

Ruddi Rodriguez-Garcia, Laurent Chesneau, Sylvain Pastezeur, Julien Roul, Marc Tramier, Jacques Pecreaux

## ► To cite this version:

Ruddi Rodriguez-Garcia, Laurent Chesneau, Sylvain Pastezeur, Julien Roul, Marc Tramier, et al.. The polarity-induced force imbalance in *Caenorhabditis elegans* embryos is caused by asymmetric binding rates of dynein to the cortex. *Molecular Biology of the Cell*, 2018, 29 (26), pp.3063-3200. 10.1091/mbc.E17-11-0653 . hal-01903171

**HAL Id: hal-01903171**

**<https://univ-rennes.hal.science/hal-01903171>**

Submitted on 9 Nov 2018

**HAL** is a multi-disciplinary open access archive for the deposit and dissemination of scientific research documents, whether they are published or not. The documents may come from teaching and research institutions in France or abroad, or from public or private research centers.

L'archive ouverte pluridisciplinaire **HAL**, est destinée au dépôt et à la diffusion de documents scientifiques de niveau recherche, publiés ou non, émanant des établissements d'enseignement et de recherche français ou étrangers, des laboratoires publics ou privés.

# The polarity-induced force imbalance in *Caenorhabditis elegans* embryos is caused by asymmetric binding rates of dynein to the cortex.

Ruddi Rodriguez-Garcia<sup>a,b,\*</sup>, Laurent Chesneau<sup>a,\*</sup>, Sylvain Pastezeur<sup>a</sup>, Julien Roul<sup>a,c</sup>, Marc Tramier<sup>a</sup>, and Jacques Pécrciaux<sup>a,†</sup>

<sup>a</sup>CNRS, Univ Rennes, IGDR (Institute of Genetics and Development of Rennes) – UMR 6290, F-35000 Rennes, France; <sup>b</sup>Present address: Cell Biology, Faculty of Science, Utrecht University, 3584 Utrecht, The Netherlands; <sup>c</sup>Present address: LAAS (Laboratoire d'analyse et d'architecture des systèmes), 31031 Toulouse, France.

\*These authors contributed equally to this work.

†Address correspondence to J.P. ([jacques.pecreux@univ-rennes1.fr](mailto:jacques.pecreux@univ-rennes1.fr)).

Abbreviations used: FCS, fluorescence correlation spectroscopy; LSP, lower spindle plane; FCCS, fluorescence cross-correlation spectroscopy; DIC, differential interference contrast; SD, standard deviation; MDCK, Madin–Darby canine kidney; FRAP, fluorescence recovery after photobleaching; SDM, standard deviation maps.

Running title: Dynamics of dynein and force polarity.

## Abstract

During asymmetric cell division, the molecular motor dynein generates cortical pulling forces which position the spindle to reflect polarity and adequately distribute cell fate determinants. In *Caenorhabditis elegans* embryos, despite a measured anteroposterior force imbalance, antibody staining failed to reveal dynein enrichment at the posterior cortex, suggesting a transient localization there. Dynein accumulates at the microtubule plus ends, indirectly binding to EBP-2<sup>EB</sup>. This accumulation, although not transporting dynein, contributes modestly to cortical forces. Most dyneins may instead diffuse to the cortex. Tracking of cortical dynein revealed two motions: one directed, and the other diffusive-like, corresponding to force-generating events. Surprisingly, while dynein is not polarized at the plus ends or in the cytoplasm, diffusive-like tracks were more frequently found at the embryo posterior tip, where the forces are higher. This asymmetry depends on GPR-1/2<sup>LGN</sup> and LIN-5<sup>NuMA</sup>, which are enriched there. In *csnk-1(RNAi)* embryos, the inverse distribution of these proteins coincides with an increased frequency of diffusive-like tracks anteriorly. Importantly, dynein cortical residence time is always symmetric. We propose that the dynein binding rate at the posterior cortex is increased, causing the polarity-reflecting force imbalance. This mechanism of control supplements the regulation of mitotic progression through the non-polarized dynein detachment rate.

## Highlight Summary for TOC

In nematode zygote mitosis, force imbalance is caused by an enhanced binding rate of dynein to the posterior cortex, in response to GPR-1/2<sup>LGN</sup> and LIN-5<sup>NuMA</sup> enrichment, and *in fine* reflects polarity. It adds to the control of mitotic progression, acting by increasing the cortical residence time (persistence) of the force generators during mitosis.

# Introduction

---

Successful symmetric and asymmetric cell division relies on the precise positioning and orientation of the mitotic spindle, which in turn ensures the correct partitioning of chromosomes and cell organelles. This choreography requires cortical pulling forces. From yeast to humans, the molecular motor dynein is key to producing these (Carminati and Stearns, 1997; Shaw *et al.*, 1997; Gonczy *et al.*, 1999; Karki and Holzbaur, 1999; Dujardin and Vallee, 2002; Nguyen-Ngoc *et al.*, 2007; Moore *et al.*, 2008; Markus and Lee, 2011b; Collins *et al.*, 2012; Laan *et al.*, 2012; Kotak and Gonczy, 2013). It localizes at the cell cortex and pulls on the astral microtubules that radiate from the spindle poles (McNally, 2013). Indeed, cytoplasmic dynein (hereafter referred to simply as “dynein”) is minus-end directed, walking toward the spindle poles.

Dynein is a dimer of a multi-subunit complex that performs various functions depending on the choice of subunits (Pfister and Lo, 2012). In *Caenorhabditis elegans*, because only one homolog of the intermediate chain of dynein DYCI-1 exists, we used a labeling of this subunit to reveal dynein in all its functions. Consistently, DYCI-1 depletion results in phenotypes that mostly reflect the loss of the heavy chain, containing the motor domain (Kamath and Ahringer, 2003; Sonnichsen *et al.*, 2005). To understand how dynein-generated forces contribute to spindle positioning, we previously analyzed spindle rocking during mitotic anaphase in *C. elegans* zygotes. Our results suggest that cortical force generators pull briefly, for 1 second or less (Pecreaux *et al.*, 2006a). This was confirmed by the direct viewing of dynein heavy chain (DHC-1) at the cortex both in nematodes and mammalian cells (Collins *et al.*, 2012; Kiyomitsu and Cheeseman, 2012; Barbosa *et al.*, 2017; Schmidt *et al.*, 2017). So with such a transient residence, how does dynein reach the cortex? In higher eukaryotes, it most likely arrives from the cytoplasm rather than from the pool at the microtubule plus ends, thus relegating plus-end accumulation to a minor role (Splinter *et al.*, 2012; Duellberg *et al.*, 2014; Barbosa *et al.*, 2017; Baumbach *et al.*, 2017; Jha *et al.*, 2017; Schmidt *et al.*, 2017). However, pulling forces may still depend weakly on plus-end tracking protein EBP-2<sup>EB</sup>, which is required for dynein accumulation. Therefore, more investigation is still needed into dynein accumulation at the plus ends, and into dynein’s role in cortical force generation.

Although it is clear that the cortical forces generated by dynein play an essential role in a broad range of organisms, the mechanistic link between polarity and these forces remains elusive (McNally, 2013). Indeed, in the *C. elegans* zygote the posterior displacement of the spindle has been attributed to polarity cue-induction of higher forces at the posterior cortex (Grill *et al.*, 2001; Colombo *et al.*, 2003; Grill *et al.*, 2003). This is caused by a doubling of the *active* force generators at the posterior cortex as compared to the anterior one (Grill *et al.*, 2003; Grill and Hyman, 2005; Pecreaux *et al.*, 2006a; Nguyen-Ngoc *et al.*, 2007; Redemann *et al.*, 2010). Besides an unequal amount of dynein at the cortex, the force imbalance could also be caused by a differential regulation of the intrinsic properties of dynein acting as a molecular motor, or of its dynamics, such as a higher binding rate or a lower unbinding rate on the stronger-force side. Importantly, the mechanism that translates polarity into a force imbalance is involved in the segregation of cell fate determinants and in the balance between proliferation and differentiation (Gonczy, 2008; Moore and Cooper, 2010; Morin and Bellaiche, 2011; McNally, 2013; Rose and Gonczy, 2014; Williams *et al.*, 2014; di Pietro *et al.*, 2016).

To explore the causes of the force imbalance, we first focused on the mechanisms for bringing dynein to the cortex. Combining advanced image processing and fluorescence correlation spectroscopy (FCS), we found that the dynein accumulated at the microtubule

plus ends in an EBP-2<sup>EB</sup>-dependent manner was not transported to the cortex. However, this dynein pool does contribute slightly to the pulling forces. Most dyneins probably reach the cortex by 3D diffusion from the cytoplasm instead. In both mechanisms, we found that the dynein inflow to the cortex was not polarized, and they could not account for the pulling force imbalance. However, by carefully analyzing the dynamics at the cortex, we did find an asymmetric binding rate of dynein to the force-generating complex. This asymmetry leads to more microtubule pulling events on the posterior side, in a polarity-dependent manner.

## Results

---

### Dynein pools in the cytoplasm are not polarized.

To determine whether cytoplasmic dynein pools could contribute to building the force imbalance at the cortex, we first investigated whether soluble dynein was symmetrically distributed in the cytoplasm. We used a strain expressing a fluorescent dynein intermediate chain, DYCI-1, labeled by mCherry expressed under its own promoter and carried by a transgene (Sarov *et al.*, 2006; Sarov *et al.*, 2012). During mitosis, this strain displayed no significant phenotype, and the corresponding transgene rescued the *dyci-1(tm4732)* null allele. So even with possibly altered expression levels, DYCI-1::mCherry performs like the native protein (Supplemental Text 1.1-2). We used spinning disc microscopy to examine the strain in a plane between the coverslip and the spindle so-called the lower spindle plane (LSP), and at the cortex (Figure 1, A-D). In the LSP, we observed both spindle and central spindle staining, with dynein spots moving towards the cortex during metaphase and anaphase (Figure 1A-B, Supplementary Figure S1A,C, and Movies S1-2). This is consistent with the spindle and dotted cytoplasmic localizations that were previously revealed after both antibody staining and live imaging of the dynein subunit DHC-1 (Gonczy *et al.*, 1999; Nguyen-Ngoc *et al.*, 2007; Barbosa *et al.*, 2017; Schmidt *et al.*, 2017). After confirming our labeling, we then checked whether the cytoplasmic dynein fraction was polarized. FCS measurements of the dynein in the cytoplasm did not show an asymmetry (Figure 1e, Supplemental Text 1.3) (Widengren *et al.*, 1994), and we concluded that equal amounts of soluble dynein are available in both embryo halves, ready to diffuse and bind to the cortex.

The unequal amounts of dynein at each cortex half could be caused by EB homolog proteins and the corresponding accumulation of dynein at the plus ends. To further investigate dynein behavior in the cytoplasm, we denoised the images, tracked the dynein spots in the LSP, and analyzed their dynamics in detail (Supplemental Figure S2A-C, Supplemental Text 2) (Sage *et al.*, 2005; Huet *et al.*, 2006; Jaqaman *et al.*, 2008; Coupe *et al.*, 2012). We mostly found directed tracks that moved from the centrosome to the cortex (Figure 1F, G). Since those moving in the reverse direction were rare ( $5 \pm 3\%$ ) and not expected to help bring dynein to the cortex, these directed tracks were not investigated further. In a similar analysis of simulated particles, we observed that short tracks tended to be classified as diffusive-like regardless of their actual motion. So, in processing experimental data, we ignored the diffusive-like tracks, being uncertain of their real motion (Supplemental Figure S3, Movie S8-9, Supplemental Text 2.5). We therefore focused only on spots displaying a directed motion toward the cortex. To ascertain that these corresponded to dyneins accumulating at the microtubule plus ends, we confirmed that the tracks depended upon end-tracking protein EBP-2<sup>EB</sup>, the dynactin subunit DNC-1<sup>p150glued</sup> and LIS-1, but not on CLIP-1<sup>CLIP170</sup> in agreement with previous findings (Supplemental Figure S4A-F, Supplemental Text 3.1) (Barbosa *et al.*, 2017; Schmidt *et al.*, 2017). EBP-2 by itself consistently displayed centrifugal spots independently of DNC-1<sup>p150glued</sup> and LIS-1,

confirming that dynein accumulates at the plus ends by interacting with these proteins, which in turn binds EBP-2 (Supplemental Figure S4G). Furthermore, the dynein spots colocalized with microtubules and EBP-2 (Figure 2A-B, Supplemental Figure S5A-D, Movies S10-11, Supplemental Text 3.2). Since these spots were therefore proven to correspond to the plus-end dyneins, we checked the symmetry of their distribution. We measured the posterior-to-anterior ratios, which were  $0.95 \pm 0.09$  for the directed tracks ( $p = 0.7$ , compared to 1), and  $1.0 \pm 0.1$  for the diffusive-like ones ( $p = 0.5$ ,  $N = 7$  embryos, 1341 tracks). In both cases, we found no significant asymmetry. Importantly, the spot intensities were similarly distributed between the anterior and posterior (Supplemental Figure S5E, Kolmogorov-Smirnov test,  $p = 0.27$ ,  $N = 8$  embryos). Thus, the dynein counts in each spot are the same for both the anterior and posterior embryo halves. Therefore, the plus-end accumulation of dynein is not polarized. To conclude, there are equal pools of dynein in the anterior and posterior cytoplasm, resulting in symmetric inflow to the cortex either by cytoplasmic diffusion or by via the microtubule plus-ends.

### Dyneins are not transported to the periphery by the microtubule plus ends.

We next wondered whether dynein accumulation at the microtubule plus ends could have a more subtle contribution to the force imbalance. Besides having larger or more numerous dynein spots on the posterior side, their dynamics could be asymmetrical, for instance if spots arrive faster to that side. Indeed, while the microtubule growth rates are similar on both sides, their residence time at the cortex was reported to be polarized (Labbe *et al.*, 2003; Srayko *et al.*, 2005). We first checked whether the amount of dynein reaching the cortex through the plus-ends is enough to contribute significantly to cortical forces. We used FCS to image the microtubule tips, finding  $\sim 50$  DYCI-1::mCherry proteins per plus-end in the strain also carrying the endogenous copies. In comparison, we counted 3-4 times more EBP-2::GFP in each plus end (Supplemental Text 1.4). Previous studies showed 100-200 microtubule contacts at the cortex at any time during anaphase (Pecreaux *et al.*, 2016; Bouvrais *et al.*, 2017; Redemann *et al.*, 2017). Therefore, dynein accumulation at the microtubule plus ends could provide a large excess of dyneins to the cortex, much higher than the previously reported 10-100 active force generators residing 1 s or less on each half cortex (Grill *et al.*, 2003; Pecreaux *et al.*, 2006a; Barbosa *et al.*, 2017; Schmidt *et al.*, 2017).

So does an accumulation of dynein at the microtubule plus ends contribute to a cortical-force imbalance? To explore this, we checked whether the dynein pool is transported to the cell periphery as it is in yeast (Sheeman *et al.*, 2003; Lee *et al.*, 2005; Markus *et al.*, 2009; Markus and Lee, 2011a; Roberts *et al.*, 2014). By FCS, we examined microtubule ends moving across the focal volume (comet tails, see Figure 2C) in a doubly labeled EBP-2::GFP;DYCI-1::mCherry strain. Both EBP-2 and DYCI-1 had similar spot association kinetics, which depend exponentially on local cytoplasmic concentrations of the corresponding proteins (Figure 2D, Supplemental Text 4.1) (Dragestein *et al.*, 2008). Furthermore, the association rates obtained by fitting were similar. Therefore, just like EBP-2<sup>EB</sup>, dynein is mostly recruited from the cytoplasm at the plus ends. Interestingly, when examining these two proteins in the cytoplasm by fluorescence cross-correlation spectroscopy (FCCS), they are not associated, which indicates that dynein attaches to the plus ends in its own way (Supplemental Figure S6A). This is reminiscent of the cortical targeting mechanism of dynein in yeast, and is thus compatible with its transport.

In contrast to yeast, dynein plus-end accumulation did not seem to be transported after an *in vitro* reconstitution using mammalian purified proteins (Duellberg *et al.*, 2014; Baumbach *et al.*, 2017; Jha *et al.*, 2017). The critical question is thus whether dynein stays on the microtubule lattice when EBP-2<sup>EB</sup> leaves the plus ends. Indeed, EB is only accumulated

there, but not transported (Bieling *et al.*, 2007). EBP-2 and DYCI-1:mCherry detachment rates were similar (Figure 2E), suggesting that dynein is not transported. To strengthen this result, we next checked whether dynein displays the same detachment dependence on microtubule growth rates as EB proteins. Indeed, the tail of the EB fluorescent comet at the plus ends grows as the microtubule grows faster. We thus measured (generally in 7 embryos, 1500 tracks per condition) the DYCI-1::mCherry comet-tails, varying the growth rates through hypomorphic *klp-7(RNAi)* and *clip-1(RNAi)*. These showed a linear relation with a slope significantly different from zero:  $1.2 \pm 0.2$  s ( $p = 0.03$ ) (Figure 2F, Supplemental Figure S6B, Supplemental Text 4.2). This result shows that most dyneins leave the microtubule plus end similarly to EBP-2<sup>EB</sup>. Therefore, like that protein, dynein is only accumulated and not transported at the microtubule plus ends. In conclusion, the force imbalance at the cortex could not be caused by an asymmetry in dynein dynamics at the plus ends.

### EBP-2 contributes modestly to cortical pulling forces

Dynein may appear in two pools at the cortex. One is dependent on LIN-5<sup>NuMA</sup>, a member of the trimeric complex that generates pulling forces, and the other is dependent on EBP-2<sup>EB</sup> and may act as a backup to the first pool to ensure cortical pulling (Schmidt *et al.*, 2017). To see whether this second pool could contribute to force imbalance, we first checked whether EBP-2<sup>EB</sup> and dynein accumulated at the plus ends contribute to cortical forces. To do so, we used  $\gamma$ TUB::GFP centrosome labeling and analyzed the oscillations of the posterior centrosome upon *ebp-1/2/3(RNAi)* or crossing with null mutation *ebp-2(gk756)*. We found that although its paralogs EBP-1 and EBP-3 do not, EBP-2 contributes a bit to force generation (Figure 3A). Could this be related to dynein accumulating at the plus ends through EBP-2? We measured the oscillation amplitudes in control and *ebp-2(gk756)* null mutants in the absence of DYCI-1, and found no significant differences (Figure 3A). As a control, we performed the same analysis in *ebp-2(gk756)* null mutant and found no significant difference with and without *clip-1<sup>CLIP170</sup>(RNAi)* treatment. These experiments suggest that EBP-2<sup>EB</sup> and DYCI-1 probably act along the same pathway. We therefore suggest that dynein accumulated at the microtubule plus ends contributes mildly to cortical pulling forces.

To strengthen this conjecture, we went at the question from a different direction, using our previously published “tube” assay. This reports the location of force-generating events by creating cytoplasmic membrane invaginations (Figure 3B) (Redemann *et al.*, 2010). These are rare in non-treated conditions, but more numerous upon weakening the actin-myosin cortex by *nmy-2(RNAi)*, done only partially to preserve the polarity (Figure S6C, Supplemental Text 5.1). PH::GFP membrane labeling reveals these invaginations. Importantly, RNAi depletion of either cortical force generators or related proteins significantly decreases invagination counts. We added *ebp-2(RNAi)* to this hypomorphic *nmy-2(RNAi)*, resulting in significantly decreased invaginations as compared to the control (Figure 3C). We thus confirmed that EBP-2 enhances cortical force generation.

It was recently suggested that EB helps initiate the dynein run, thus in our case generating cortical forces. We therefore decided to address whether EBP-2 promotes dynein targeting to the cortex by measuring dynein after EBP-2 depletion. However, first, we had to ensure that the DYCI-1::mCherry visible as transient spots at the cortex is involved in force-generating events (Figure 1C, Supplemental Figure S1E and G, and Movie S3). We began by using the tube assay and crossed the DYCI-1::mCherry and PH::GFP strains, observing the cortex upon partial *nmy-2(RNAi)* (Movie S6, Figure 3D-E). We found that half of the invaginations colocalized with DYCI-1::mCherry spots (Figure 3F and Supplemental Text 5.1). We figured that the lack of colocalization in the other half was because of detection

limits imposed by high DYCI-1::mCherry cytoplasmic background fluorescence, and indeed the threshold for spot detection over the background fluorescence was estimated at  $26 \pm 4$  dyneins per spot (Supplemental Text 2.6 and Supplemental Figure S8). We also noticed that dynein spots appeared 0.4 s before invagination, suggesting that pulling forces created by labeled dyneins must generate the invaginations (Figure 3D-E and Movie S7). To reinforce our hypothesis, we asked whether labeled DYCI-1 colocalizes with the members of the cortical force-generating complex GPR-1/2 (Nguyen-Ngoc *et al.*, 2007). We crossed strains carrying randomly integrated DYCI-1::mCherry and GPR-1::YFP and acquired images of both dyes. We found that 30% of the cortical spots in DYCI-1::mCherry ( $N = 8$  embryos) colocalized with GPR-1::YFP ones (Figure 3G, Supplemental Text 3.2). Because there are a limited number of dynein cortical anchors, not all DYCI-1::mCherry spots are likely to contribute to pulling forces, and thus this colocalization proportion is coherent (Grill and Hyman, 2005; Pecreaux *et al.*, 2006a; Park and Rose, 2008; Riche *et al.*, 2013). Next, we did RNA interference to partially deplete the dynein light chain DLI-1, known to be involved in cortical pulling forces, resulting in an almost complete disappearance of the DYCI-1::mCherry spots at the cortex (Figure 3H) (Yoder and Han, 2001; Pecreaux *et al.*, 2006a). Overall, DYCI-1::mCherry thus clearly reveals the dyneins is involved in force generation at the cortex.

Having ascertained that cortical DYCI-1::mCherry spots correspond to force generators, we observed them on depleting EBP-2 either by *ebp-2(RNAi)* or by crossing with the null *ebp-2* mutant (Figure 3I-J). We found a drastic reduction in both diffusive-like and directed cortical track densities (Figure 3K), similar to what happens in the lower spindle plane upon EBP-2 depletion. Together with the results based on the posterior centrosomal oscillations, we suggest that EBP-2 may contribute, albeit modestly, to targeting dynein to the cortex and to pulling force generation there. EBP-2's limited contribution makes it unlikely that it plays a part in the anteroposterior imbalance of forces at the cortex.

### Dynein dynamics at the cell cortex.

To further exclude that EBP-2 contributes to creating the force imbalance, we analyzed the dynamics of dynein at the cortex as we did in the LSP, finding equal proportions of directed and diffusive-like tracks (Figure 4A-B). Furthermore, spots of both types spent less than 1 s at the cortex (Figure 4C-D and Supplemental Text 6.1). Since dynein spots mostly display a directed motion in the cytoplasm, we reasoned that cortical directed tracks might correspond to dynein spots completing their arrival to the cortex. Indeed, the optical sectioning in spinning disc microscopes may allow for viewing of the sub-cortical regions. To test this hypothesis, we used RNAi to deplete EFA-6, a putative microtubule regulator whose depletion results in more stable microtubules which are more numerous at the cortex. Upon *efa-6(RNAi)*, we found more directed tracks than in the control, while the diffusive-like population was not significantly affected (Figure 4E-F). Therefore, we concluded that directed tracks should correspond to dynein at the plus ends of microtubules. In this respect, these tracks belong to the EBP-2-dependent population of cortical dynein (Schmidt *et al.*, 2017). Because the dyneins move in the same way as those in the LSP, which is not polarized, we can conclude that they do not contribute to the cortical force imbalance.

### Cortical dynein spots with diffusive-like motion display an asymmetric distribution which is polarity-dependent.

To further understand how polarity translates into force imbalance, we checked whether the population having diffusive-like motion could be dynein residing at the cortex, engaged in pulling-force generation. We analyzed the motion of dynein spots within four regions extending equally along the AP-axis and measured the number of tracks per unit of time,

also known as the frequency (Figure 5D, Supplemental Text 2.4), which is independent of the dynein residence time at the cortex. To account for dynein expression level variability (Supplemental Text 2.4), we normalized to the average value of the anterior-most region (#1 in Figure 5D) in the control. We observed that only the spots with a diffusive-like motion were polarized (Figure 5A-B). Because the frequencies in the middle regions were symmetric and forces from these regions were suggested to have smaller contributions to spindle positioning, we concentrated only on the outside regions (1 and 4 in Figure 5D) (Krueger *et al.*, 2010). We reasoned that since GPR-1/2<sup>LG<sup>N</sup></sup> is posited to be the limiting factor in force generation, its depletion should alter the diffusive-like track counts (Colombo *et al.*, 2003; Park and Rose, 2008; Riche *et al.*, 2013). We measured their frequency in embryos subjected to *gpr-1/2(RNAi)* and found that it was lower than in the control (Figure 5E). Furthermore, this treatment also suppressed the asymmetry (Figure 5F). Although partial, this treatment was penetrant, since another experiment using differential interference contrast (DIC) microscopy showed a total disappearance of posterior centrosomal oscillations under the same conditions ( $N = 7$  embryos), while they remained in the  $N = 8$  untreated controls as previously observed (Colombo *et al.*, 2003). Importantly, the *gpr-1/2(RNAi)* treatment preserved a posterior displacement that was indistinguishable from the control, with a final centrosomal position at  $76 \pm 7\%$  of embryo length (mean  $\pm$  SD) compared to  $79 \pm 1\%$  in the control, thus the positional regulation of forces was normal (Riche *et al.*, 2013; Bouvrais *et al.*, 2017). The following treatments were also partial in order to preserve a spindle positioning indistinguishable from the control. Overall, we concluded that the diffusive-like population consists of dynein involved in cortical pulling, and does reveal force-generating events.

Because equal flows of dynein reach the cortex from the anterior and posterior cytoplasm, only three mechanisms can account for the force asymmetry: (1) the binding rate of dynein to the cortex is higher on posterior side; (2) dynein resides on and pulls longer on posterior side; or (3) dynein is more efficient on posterior side (e.g. develops higher forces on that side). This last option appears unlikely, since it fails to account for the asymmetric frequencies of diffusive-like tracks or for the asymmetric number of active force generators (Figure 5A) (Grill *et al.*, 2003). We wondered which alternative would best explain the differences in the anterior and posterior centrosomal oscillations. We examined non-treated embryos carrying  $\gamma$ TUB::GFP, and found that the frequencies and amplitudes on the posterior side were both greater than those of the anterior one. We compared these results with the predictions of the model from our previous work (Pecreaux *et al.*, 2006a), using these three possibilities (Supplemental Text 6.2). In fact, we found that the experimental oscillations were consistent with an asymmetry in dynein dynamics, either in the binding or unbinding rates (possibilities 1 and 2). But they were not consistent with asymmetric efficiency (#3), or even with unequal total dynein counts caused by an asymmetric inflow to the cortex. We thus set out to investigate the possibilities tied to dynein dynamics. However, because the model is linearized and the experimental frequencies of centrosomal oscillations are moderately different, we could not yet choose between the other two explanations.

We next used direct viewing of force-generating events to decide whether dynein binds to the cortex at a higher rate on posterior or whether it stays there longer (alternatives #1 and #2, respectively). We measured the dynein spot residence time, and found no significant differences between the posterior and anterior regions for the diffusive-like population (Supplemental Text 6.1, Figure 5C-D). This supports an asymmetry in binding rates (alternative #1). Furthermore, we observed that *gpr-1/2<sup>LG<sup>N</sup></sup>(RNAi)* suppressed the asymmetry in the diffusive-like track frequencies while only slightly decreasing the residence time. To gain certainty, we targeted the force-generating complex in another fashion, partially depleting LIN-5<sup>NuMA</sup> by RNAi (Figure 5H) (Gotta *et al.*, 2003; Nguyen-

Ngoc *et al.*, 2007). This treatment suppressed the asymmetric frequencies of the tracks having a diffusive-like motion, while not significantly altering their residence times (Figure 5F,H). However, to ensure correct meiosis we were limited to a more hypomorphic treatment since LIN-5 is involved in more functions than GPR-1/2 is (van der Voet *et al.*, 2009). As above, we checked that the final spindle positioning was not significantly affected by measuring the position at which the cytokinesis furrow started to ingress at the cortex. This was  $55.6 \pm 2.1\%$  (mean  $\pm$  SD,  $N = 5$ ) upon *lin-5(RNAi)*, compared to the control's  $59.0 \pm 3.9\%$  ( $N = 9$ ,  $p = 0.24$ ). Together, these experiments support the idea that polarity is reflected by an increase in dynein binding to the cortex on the posterior side.

Finally, we asked whether GPR-1/2 enrichment at the posterior pole could cause the enhanced binding rates. We altered its localization and investigated the frequency distribution of the diffusive-like tracks. Indeed, upon *cnsk-1(RNAi)*, GPR-1/2 and LIN-5 are enriched at the anterior pole of the embryo during early mitosis, then homogeneously distributed later on (Panbianco *et al.*, 2008). Upon *cnsk-1(RNAi)*, hypomorphic to preserve the spindle position, we observed the cortex and analyzed the dynein spots during metaphase. We found a significant increase in the frequency at the anterior pole as compared to the control, canceling the asymmetry (Figure 5G). As expected, the residence times of the same dynein spots were unaffected (Figure 5I). Using DIC at the mid-plane, we ensured that the treatment did not alter the position for ingression of cytokinesis furrows at the cortex. We found  $56.4 \pm 2.5\%$  (mean  $\pm$  SD,  $N = 4$ ) upon *cnsk-1(RNAi)*, compared to  $59.0 \pm 3.9\%$  ( $N = 9$ ,  $p = 0.24$ ) in the control. Therefore, the GPR-1/2<sup>LGN</sup> and LIN-5<sup>NuMA</sup> concentrations are reflected in the dynein binding rate variations. Overall, direct observation of the dynein population displaying diffusive-like motion led us to conclude that the force imbalance is caused by a larger binding rate on the posterior side. This increase is probably due to the presence of larger concentrations of either GPR-1/2 or LIN-5 at the cortex.

## Discussion

---

Using a fluorescence-labeled DYCI-1 as a *bona fide* reporter of dynein, we discovered that this molecular motor is not actively transported towards the cell periphery. Instead it accumulates at the microtubule plus ends, and is only briefly immobilized on their lattice. The lack of EBP-2<sup>EB</sup> mildly but significantly decreases cortical forces, however. It was proposed that cortical forces may position the spindle independently of dynein using hypomorphic RNA interference or temperature-sensitive alleles of dynein heavy chain DHC-1 (Schmidt *et al.*, 2005). However, some dynein activity may have persisted in these experiments, leaving open the possibility that dynein is strictly necessary to move the spindle to the posterior side. Consistently, a partial *dli-1(RNAi)* cancels out centrosomal oscillations and strongly reduces posterior displacement, suggesting that dynein contributes to most if not all cortical pulling force generation (this work and (Yoder and Han, 2001; Pecreaux *et al.*, 2006a). More recently, using laser severing of the spindle, a reduced peak velocity was observed upon *ebp-2(RNAi)* (Schmidt *et al.*, 2017). Surprisingly, using an *ebp-2* null mutant obtained by CRISPR-Cas9 and tracking the centrosomes in DIC at one frame every 2 seconds, the same authors failed to observe the subtle anaphase decrease in oscillation amplitude. In contrast, we were able to see it using both *ebp-2(RNAi)* and the *ebp-2(qk756)* null mutant. To account for this discrepancy, these authors suggest that a pool of dynein dependent on EBP-2 and located at the microtubule plus ends creates a backup mechanism to ensure cortical pulling force generation. Alternately, this discrepancy might be due to the reduced time resolution of their centrosomal tracking assay. We confirmed

our results, observing fewer membrane invaginations upon *ebp-2(RNAi)*. In sum, it seems clear that EBP-2 plays a role, although modest, in cortical force generation.

### Putative mechanisms for the role of EBP-2<sup>EB</sup>

When EBP-2<sup>EB</sup> is depleted, there are fewer dynein spots at the cortex. This suggests that this protein contributes to the cortical localization of dynein, consistent with previous reports (Barbosa *et al.*, 2017; Schmidt *et al.*, 2017). However, surprisingly, depleting EBP-2<sup>EB</sup> only mildly reduces cortical forces. So how does EBP-2 act? In light of recent studies, its mechanisms are threefold: increasing dynein targeting of the cortex; promoting the assembly of the force-generating complex; and initiating the dynein run to the minus ends.

During microtubule growth, an EBP-2-dependent accumulation of dynein could bias its diffusion towards the periphery. Indeed, when EBP-2 and thus dynein detach from GDP-tubulin behind the cap, dynein affinity for the EBP-2 bound to the GTP-cap may encourage its diffusion toward the plus ends, i.e. towards the cell periphery (Rousselet *et al.*, 1994; Preciado Lopez *et al.*, 2014). We consistently found that dynein and EBP-2 did not associate in the cytoplasm. Although not very efficient, a subtle mechanism such as this could promote cortical targeting in the context of fast dynein turnover.

At the cortex, having concentrated dyneins at the microtubule plus ends would facilitate the assembly of the force-generating complex together with GPR-1/2 and LIN-5, and the capture of a microtubule for it to pull on. Such an advantage would be even stronger if the force generators act in clusters, as recently suggested using human purified proteins, and also if dynein targeting to the cortex by diffusion is reduced (Okumura *et al.*, 2018). This reduction could occur when the sub-cortical dynein concentration decreases as dynein leaves the cortex and runs along the microtubules to the centrosome, as in MCDK mammalian cells (Zheng *et al.*, 2013). These findings in other organisms call for further studies to elucidate the details of offloading in the nematode.

Finally, once the complex has assembled and has engaged a microtubule, EBP-2<sup>EB</sup> may enhance the initiation of the dynein run and thus force generation. This mechanism was previously reported *in vitro* using human proteins and in the nematode (Barbosa *et al.*, 2017; Jha *et al.*, 2017). EBP-2 can also promote the tracking of depolymerizing microtubule ends by dynein, a supplemental mechanism for force generation also proposed in *C. elegans* (Kozłowski *et al.*, 2007; Laan *et al.*, 2012; Duellberg *et al.*, 2014; Baumbach *et al.*, 2017; Okumura *et al.*, 2018). Even disregarding these mechanistic details, it is clear that the majority of the dynein-dependent forces are still present if EBP-2<sup>EB</sup> and even all three EBP-1/-2/-3 orthologs are absent (Schmidt *et al.*, 2017); and this study). Therefore, we suggest that neither these mechanisms nor the cytoplasmic diffusion of dynein play a role in building the imbalance of cortical forces reflecting embryo polarity.

### The diffusive-like population at the cortex reports force-generating events.

We found two populations of dynein at the cortex, with distinct spot dynamics. Only the one with diffusive-like motion is asymmetrically distributed. Using fluorescence recovery after photobleaching (FRAP), Schmidt and colleagues consistently found that only their LIN-5-dependent dynein population displayed different dynamics between the anterior and posterior cortices, not their EBP-2-dependent one (Schmidt *et al.*, 2017). These populations may well correspond to our tracks with diffusive-like and directed motions. Furthermore, we found that spots with a diffusive-like motion reveal force-generating events. In support of this hypothesis and in addition to their dependence on GPR-1/2 and LIN-5, their residence times are consistent with the brief cortical stay of microtubules engaged in force

generating and with the estimated force-generator runtimes deduced from the modelling of centrosomal oscillations during anaphase (Pecreaux *et al.*, 2006a; Kozlowski *et al.*, 2007; Bouvrais *et al.*, 2017; Sugioka *et al.*, 2018). Secondly, the number of spots is consistent with the expected active force-generator count: 10-100 per cortex half (Grill *et al.*, 2003; Redemann *et al.*, 2010). Indeed, in the posterior region, we observed approximately 0.008 diffusive-like tracks per  $\mu\text{m}^2$  of visible cortex area (instantaneous density). This extrapolates to about 20 diffusive-like tracks in the posterior half at any instant, which is well within the published range.

The force-generating events come from dynein having diffusive-like motion, and we wonder whether some spots in this population may relate to other mechanisms. Firstly, it is possible that some spots represent stalled dyneins (Laan *et al.*, 2012). This would be consistent with the fact that GPR-1/2 colocalizes with only a third of all dynein spots (equal proportions of diffusive-like and directed, so we would have expected about 50% colocalization). However, the number of stalled dyneins must be low, as a detailed analysis of centrosomal motion does not detect them (Pecreaux *et al.*, 2016). Secondly, some tracks might mix motions that are directed (microtubules arriving at the cortex) and diffusive-like (dynein taking part in force generation), and are classified according to where they spent the longest time. These two considerations may account for why we observed a posterior-to-anterior ratio of dynein-track frequencies below 2, when it has been proposed that there are double the active force generators present at the posterior pole (Grill *et al.*, 2003). However, since the diffusive-like population mostly corresponds to force-generating events, this offers a unique opportunity for deciphering the details of the polarity-induced force imbalance.

### The mechanism of the polarity-reflecting force imbalance

After studying cytoplasmic dynein, we ruled out that a different number of molecules reaches each half-cortex. We instead suggest that the force imbalance is caused by dynein's higher binding rate at the posterior cortex (Figure 6). Previous investigations reported an anteroposterior asymmetry in cortical residence time of the microtubules, although the low frame rates used (0.5 and 1.4 Hz, respectively) limited the resolution (Labbe *et al.*, 2003; Sugioka *et al.*, 2018). Furthermore, these authors found surprisingly long residence times as compared to established values (Kozlowski *et al.*, 2007; Bouvrais *et al.*, 2017). It is possible that a low-performance linker in the tracking algorithm would lead to incorrect analysis of closely packed successive tracks, interpreting them as the same spot. Such an artefact would take spot frequency imbalances and present it as residency imbalances.

What mechanism could yield higher binding rates of dynein at the posterior cortex? Certainly higher amounts of GPR-1/2<sup>LGN</sup> or LIN-5<sup>NuMA</sup> there could displace the association/dissociation balance towards more assembly/force-generating (Figure 6). Such a mechanism does not lead to increased dynein residence at the cortex. Furthermore, it enables fast adaption to internal evolution and to dynamic polarity cues (Thery *et al.*, 2006; Fink *et al.*, 2011; Riche *et al.*, 2013; Bouvrais *et al.*, 2017). The increased binding rate could correspond not just to the kinetics of dynein associating with GPR-1/2 and LIN-5, or to the capture rate of an astral microtubule by the complex, but also to the initiation rate of the dynein force generation. In this respect, it is an effective binding rate.

This mechanism translating polarity into force imbalance is part of the threefold regulation of the forces positioning the mitotic spindle. It occurs as reported here through polarity, through spindle pole positioning (Riche *et al.*, 2013; Bouvrais *et al.*, 2017), and also through force-generator persistence in pulling on microtubules (processivity) (Pecreaux *et al.*, 2006a). This last regulation is visible as the residence time in our experiments, and is probably controlled by mitotic progression (McCarthy Campbell *et al.*, 2009). Investigating

the one-cell nematode embryo has paved the way to understanding the mechanisms of asymmetrical division (Gonczy, 2008; Morin and Bellaiche, 2011). It would be very interesting to explore whether force polarization is due to asymmetric force generator binding rates in other organisms, since these mechanisms based on dynamics are advantageous, promoting adaptation during mitosis.

## Materials and Methods

---

### Culturing *C. elegans*

*C. elegans* strains were cultured as described in (Brenner, 1974) and dissected to obtain embryos. All strains containing DYCI-1::mCherry or TBA-2<sup>α-tubulin</sup>::YFP were kept at 25°C, while functional experiments (anaphase oscillations) investigating the role of CLIP170, DLI-1, DYCI-1, and EB1 homologs were performed at 18°C. The exception to this were strains carrying *clip-1(gk470)*, kept at 23°C.

### *C. elegans* strains

The standard wild-type strain was Bristol N2 (Brenner, 1974). The following fluorescent strains were used: TH163 (DYCI-1::mCherry) (Sarov *et al.*, 2006); TH27 (GFP::TBG-1) (Oegema *et al.*, 2001); TH65 (YFP::TBA-2) (Kozłowski *et al.*, 2007); TH66 (GFP::EBP-2) (Srayko *et al.*, 2005); DE74 (GFP::PLCδ1-PH) (Johnston *et al.*, 2010); TH110 (mCherry::PAR-6) (Schonegg *et al.*, 2007); and TH242 (GPR-1::YFP) (Redemann *et al.*, 2011). Standard genetic crosses were done to generate these multi-labeled combinations: JEP2 (DYCI-1::mCherry;YFP::TBA-2); JEP12 (DYCI-1::mCherry;GFP::EBP-2); JEP20 (DYCI-1::mCherry;GFP::PLCδ1-PH) and JEP58 (DYCI-1::mCherry;YFP::GPR-1). To obtain JEP27 and JEP32 carrying the GFP::TBG-1 transgene and the *ebp-2(gk756)* or *clip-1(gk470)* mutations, we crossed TH27 with VC1614 or VC1071, respectively (*C. elegans* Deletion Mutant Consortium, 2012). The strain carrying the *dyci-1(tm4732)* lethal mutation was provided by the Mitani Lab via the National BioResource Project, and JEP9 was generated by crossing with VC2542 to balance the lethal mutation with the nT1[qIS51] translocation. JEP30 and JEP40 strains homozygous for *dyci-1(tm4732)* were obtained by double-crossing JEP9 with JEP23 and TH163, respectively (Supplemental Text 1.2). The transgenes encoding the GFP, YFP, and mCherry fusion proteins in all constructs but DYCI-1::mCherry were under the control of the *pie-1* promoter.

### Gene silencing by RNA interference

Except when otherwise stated, embryonic RNAi was done by feeding, using both the Ahringer library (Fire *et al.*, 1998; Kamath and Ahringer, 2003) and clones ordered from Source BioScience. However, the clone targeting *ebp-1/3* was made in the lab. To do so, N2 genomic DNA was used to amplify a region from the target gene (see Table 1). This amplicon was then cloned into the L4440 RNAi feeding vector and transformed into HT115 bacteria. For *ebp-1*, a region corresponding to exons 2 and 3 after splicing was amplified using four long primers and fused by PCR amplification before L4440 cloning.

**Table 1: Primers used.**

For *ebp-1* and *ebp-1/3* RNAi treatment, Q-RT-PCR measurements showed a 40–60% reduction in the number of transcripts without changes in the *ebp-2* mRNA levels. Total RNA was extracted from about 20 worms using a Direct-zol RNA MicroPrep kit (Zymo Research). Production of cDNA was done with a ProtoScript II First Strand cDNA

Synthesis kit (New England Biolabs). For Q-PCR, Power SYBR Green PCR Master Mix (Thermo Fisher Scientific) was used with a 7900HT Fast Real-Time PCR System (Applied Biosystems).

In the strains where the DYCI-1::mCherry was randomly integrated, its expression levels varied. To account for this, each RNAi experiment was compared or normalized to non-treated or L4440-treated control embryos imaged on the same day.

Except where otherwise stated, RNA interference was partial, and observation was performed 23-25 hr after plating the worms. To avoid too strong or unrelated phenotypes, we used the following treatment durations when observing the TH163 randomly integrated DYCI-1::mCherry strain: *lin-5(RNAi)*, 17 hr; *gpr-1/2(RNAi)*, 48 hr; *lis-1(RNAi)*, 16-18 hr; *dnc-1(RNAi)*, 16-18 hr; *ebp-2(RNAi)*, 20 hr; *dyci-1(RNAi)*, 16 hr; *dli-1(RNAi)* 24 hr; and *csnk-1(RNAi)*, 8 hr. To perform the “tube assay” (Redemann *et al.*, 2010), embryos were treated by *nmy-2(RNAi)* for 24 hr. In the case of double RNAi experiments for invagination counting, JEP20 L1 or L2 worms were fed over 32 hr by bacteria with the plasmid for *ebp-2(RNAi)* or with L4440 empty vector (as a control), then plated on a bacterial culture containing the two clones to perform either *ebp-2(RNAi)/nmy-2(RNAi)* or *L4440(RNAi)/nmy-2(RNAi)* by feeding for an additional 16h.

### Live imaging

Embryos were dissected in M9 buffer and mounted on pads (2% w/v agarose, 0.6% w/v NaCl, 4% w/v sucrose). We imaged one-cell *C. elegans* embryos during metaphase and anaphase. Dynein/EBP-2 tracking was performed on a LEICA DMi6000/Yokogawa CSU-X1 M1 spinning disc microscope with an HCX Plan APO 100x/1.40 Oil objective. Illumination was done with a homemade setup based on a Fianium white light laser conveniently filtered around 488 nm and 561 nm (Roul *et al.*, 2015). Except when otherwise stated, images were acquired with a 200 ms exposure time (5 Hz) using a Photometrics Evolve Camera (Roper) and MetaMorph software (Molecular Devices) without binning. During the experiments, the embryos were kept at 24°C. To image embryos at the LSP, we typically moved the focus between 3 and 5  $\mu\text{m}$  below the spindle plane (Supplemental Figure S1D). For invagination analysis, DYCI-1::mCherry and GFP::PLC $\delta$ 1-PH signals were acquired with a 168 ms exposure time at a final frequency of 2.5 Hz for each color using a Photometrics Evolve Camera on a LEICA DMi8/Yokogawa CSU-X1 M1 spinning disc microscope and Inscoper software (Inscoper, France).

### Image processing

The standard deviation maps (SDMs) were generated with Fiji's ZProject plugin for ImageJ, specifying a “standard deviation” over 6 s of the time-lapse image sequence (Rostampour *et al.*, 1988; Cai *et al.*, 2007).

The tracking of labeled centrosomes and analysis of trajectories were performed using custom tracking software (Pecreaux *et al.*, 2006a) and developed with Matlab (The MathWorks). Tracking of -20°C methanol-fixed  $\gamma$ TUB::GFP embryos indicated an accuracy of 10 nm. Embryo orientations and centers were obtained by cross-correlating embryo background cytoplasmic fluorescence with artificial binary images mimicking embryos, or by contour detection of the cell using the background fluorescence of cytoplasmic  $\gamma$ TUB::GFP with the help of an active contour algorithm (Pecreaux *et al.*, 2006b). We averaged the results over all of the replicas for each condition.

Invaginations were counted manually using ImageJ for two min after anaphase onset and were obtained by monitoring the spindle after DYCI-1::mCherry labeling.

## Statistics

The displayed center values are the means except when otherwise stated. Averaged values were compared using a two-tailed Student's *t*-test with the Welch-Satterthwaite correction for unequal variance except if stated otherwise. For the sake of simplicity, we encoded confidence levels using stars as follows: ♦,  $p < 0.1$ ; \*,  $p \leq 0.05$ ; \*\*,  $p \leq 0.01$ ; \*\*\*,  $p \leq 0.001$ ; \*\*\*\*,  $p \leq 0.0001$ ; and ns, non-significant,  $p > 0.1$ . The ns indication may be omitted for clarity's sake. We abbreviated standard deviation (SD); standard error (s.e.); and standard error of the mean (s.e.m.).

# Acknowledgments

---

We thank Prof. A.A. Hyman and Dr. M. Sarov for providing strains, in particular the kind gift of the randomly integrated DYCI-1::mCherry TH163; Dr. J.W. Dennis for the DE74 strain; Dr. S. Redemann for preliminary data on this project; Drs. N. Monnier and M. Bathes for support with analysis; Dr. G. Michaux and Prof. P. Gönczy for the feeding clones; and Drs. C. Prigent, B. Mercat, A. Pacquelet, X. Pinson, H. Bouvrais, Y. Le Cunff, G. Michaux, R. Le Borgne, and S. Huet for technical help, critical comments on the manuscript, and project discussions. Some strains were provided by the CGC, which is funded by the NIH Office of Research Infrastructure Programs (P40 OD010440; University of Minnesota, USA), by the National BioResource Project (Tokyo University, Japan), and by the *C. elegans* Gene Knockout Consortium. The MosSci strain was made by the UMS 3421 Biology of *Caenorhabditis elegans* facility, CNRS/UCBL (Lyon, France). Microscopy imaging was performed at the MRC facility, UMS 3480 CNRS/US 18 INSERM/University of Rennes 1. The FCS microscopy setup was funded by ARC grant #EML20110602452, and the spinning disc microscopy was funded by the CNRS, Rennes Métropole, and Region Bretagne (AniDyn-MT grant). We thank Inscoper for the development of fast two-color spinning disc microscopy imaging. R.R.G. and J.P. were supported by a CNRS ATIP starting grant and La Ligue Nationale Contre le Cancer. We also acknowledge *plan cancer* grant BIO2013-02 and COST EU action BM1408 (GENiE).

# Author Contributions

---

R.R.G., L.C., and J.P. designed the research, analyzed the data, and wrote the paper. R.R.G., L.C., and S.P. performed the research. J.R. and M.T. contributed new analytic tools.

# References

---

- Barbosa, D.J., Duro, J., Prevo, B., Cheerambathur, D.K., Carvalho, A.X., and Gassmann, R. (2017). Dynactin binding to tyrosinated microtubules promotes centrosome centration in *C. elegans* by enhancing dynein-mediated organelle transport. *PLoS Genet* *13*, e1006941.
- Baumbach, J., Murthy, A., McClintock, M.A., Dix, C.I., Zalyte, R., Hoang, H.T., and Bullock, S.L. (2017). Lissencephaly-1 is a context-dependent regulator of the human dynein complex. *eLife* *6*, e21768.
- Bieling, P., Laan, L., Schek, H., Munteanu, E.L., Sandblad, L., Dogterom, M., Brunner, D., and Surrey, T. (2007). Reconstitution of a microtubule plus-end tracking system *in vitro*. *Nature* *450*, 1100-1105.
- Bouvrais, H., Chesneau, L., Pastezeur, S., Delattre, M., and Pecreaux, J. (2017). Astral microtubule dynamics regulate anaphase oscillation onset and set a robust final position of the *C. elegans* zygote spindle. *bioRxiv*, 103937.
- Brenner, S. (1974). The genetics of *Caenorhabditis elegans*. *Genetics* *77*, 71-94.
- C. elegans* Deletion Mutant Consortium. (2012). Large-scale screening for targeted knockouts in the *Caenorhabditis elegans* genome. *G3* *2*, 1415-1425.
- Cai, D., Verhey, K.J., and Meyhofer, E. (2007). Tracking single Kinesin molecules in the cytoplasm of mammalian cells. *Biophys J* *92*, 4137-4144.
- Carminati, J.L., and Stearns, T. (1997). Microtubules orient the mitotic spindle in yeast through dynein-dependent interactions with the cell cortex. *J Cell Biol* *138*, 629-641.
- Collins, E.S., Balchand, S.K., Faraci, J.L., Wadsworth, P., and Lee, W.L. (2012). Cell cycle-regulated cortical dynein/dynactin promotes symmetric cell division by differential pole motion in anaphase. *Mol Biol Cell* *23*, 3380-3390.
- Colombo, K., Grill, S.W., Kimple, R.J., Willard, F.S., Siderovski, D.P., and Gonczy, P. (2003). Translation of polarity cues into asymmetric spindle positioning in *Caenorhabditis elegans* embryos. *Science* *300*, 1957-1961.
- Coupe, P., Munz, M., Manjon, J.V., Ruthazer, E.S., and Collins, D.L. (2012). A CANDLE for a deeper *in vivo* insight. *Medical Image Analysis* *16*, 849-864.
- di Pietro, F., Echard, A., and Morin, X. (2016). Regulation of mitotic spindle orientation: an integrated view. *EMBO reports* *17*, 1106-1130.
- Dragestein, K.A., van Cappellen, W.A., van Haren, J., Tsiibidis, G.D., Akhmanova, A., Knoch, T.A., Grosveld, F., and Galjart, N. (2008). Dynamic behavior of GFP-CLIP-170 reveals fast protein turnover on microtubule plus ends. *J Cell Biol* *180*, 729-737.
- Duellberg, C., Trokter, M., Jha, R., Sen, I., Steinmetz, M.O., and Surrey, T. (2014). Reconstitution of a hierarchical +TIP interaction network controlling microtubule end tracking of dynein. *Nat Cell Biol* *16*, 804-811.
- Dujardin, D.L., and Vallee, R.B. (2002). Dynein at the cortex. *Current Opinion in Cell Biology* *14*, 44-49.

- Fink, J., Carpi, N., Betz, T., Betard, A., Chebah, M., Azioune, A., Bornens, M., Sykes, C., Fetler, L., Cuvelier, D., and Piel, M. (2011). External forces control mitotic spindle positioning. *Nat Cell Biol* *13*, 771-778.
- Fire, A., Xu, S., Montgomery, M.K., Kostas, S.A., Driver, S.E., and Mello, C.C. (1998). Potent and specific genetic interference by double-stranded RNA in *Caenorhabditis elegans*. *Nature* *391*, 806-811.
- Gonczy, P. (2008). Mechanisms of asymmetric cell division: flies and worms pave the way. *Nat Rev Mol Cell Biol* *9*, 355-366.
- Gonczy, P., Pichler, S., Kirkham, M., and Hyman, A.A. (1999). Cytoplasmic dynein is required for distinct aspects of MTOC positioning, including centrosome separation, in the one cell stage *Caenorhabditis elegans* embryo. *Journal of Cell Biology* *147*, 135-150.
- Gotta, M., Dong, Y., Peterson, Y.K., Lanier, S.M., and Ahringer, J. (2003). Asymmetrically distributed *C. elegans* homologs of AGS3/PINS control spindle position in the early embryo. *Curr Biol* *13*, 1029-1037.
- Grill, S.W., Gonczy, P., Stelzer, E.H., and Hyman, A.A. (2001). Polarity controls forces governing asymmetric spindle positioning in the *Caenorhabditis elegans* embryo. *Nature* *409*, 630-633.
- Grill, S.W., Howard, J., Schaffer, E., Stelzer, E.H., and Hyman, A.A. (2003). The distribution of active force generators controls mitotic spindle position. *Science* *301*, 518-521.
- Grill, S.W., and Hyman, A.A. (2005). Spindle positioning by cortical pulling forces. *Dev Cell* *8*, 461-465.
- Huet, S., Karatekin, E., Tran, V.S., Fanget, I., Cribier, S., and Henry, J.P. (2006). Analysis of transient behavior in complex trajectories: application to secretory vesicle dynamics. *Biophysical Journal* *91*, 3542-3559.
- Jaqaman, K., Loerke, D., Mettlen, M., Kuwata, H., Grinstein, S., Schmid, S.L., and Danuser, G. (2008). Robust single-particle tracking in live-cell time-lapse sequences. *Nat Methods* *5*, 695-702.
- Jha, R., Roostalu, J., Cade, N.I., Trokter, M., and Surrey, T. (2017). Combinatorial regulation of the balance between dynein microtubule end accumulation and initiation of directed motility. *EMBO J* *36*, 3387-3404.
- Johnston, W.L., Krizus, A., and Dennis, J.W. (2010). Eggshell chitin and chitin-interacting proteins prevent polyspermy in *C. elegans*. *Curr Biol* *20*, 1932-1937.
- Kamath, R.S., and Ahringer, J. (2003). Genome-wide RNAi screening in *Caenorhabditis elegans*. *Methods* *30*, 313-321.
- Karki, S., and Holzbaur, E.L. (1999). Cytoplasmic dynein and dynactin in cell division and intracellular transport. *Curr Opin Cell Biol* *11*, 45-53.
- Kiyomitsu, T., and Cheeseman, I.M. (2012). Chromosome- and spindle-pole-derived signals generate an intrinsic code for spindle position and orientation. *Nat Cell Biol* *14*, 311-317.
- Kotak, S., and Gonczy, P. (2013). Mechanisms of spindle positioning: cortical force generators in the limelight. *Curr Opin Cell Biol* *25*, 741-748.

- Kozlowski, C., Srayko, M., and Nedelec, F. (2007). Cortical microtubule contacts position the spindle in *C. elegans* embryos. *Cell* *129*, 499-510.
- Krueger, L.E., Wu, J.C., Tsou, M.F., and Rose, L.S. (2010). LET-99 inhibits lateral posterior pulling forces during asymmetric spindle elongation in *C. elegans* embryos. *J Cell Biol* *189*, 481-495.
- Laan, L., Pavin, N., Husson, J., Romet-Lemonne, G., van Duijn, M., Lopez, M.P., Vale, R.D., Julicher, F., Reck-Peterson, S.L., and Dogterom, M. (2012). Cortical dynein controls microtubule dynamics to generate pulling forces that position microtubule asters. *Cell* *148*, 502-514.
- Labbe, J.C., Maddox, P.S., Salmon, E.D., and Goldstein, B. (2003). PAR proteins regulate microtubule dynamics at the cell cortex in *C. elegans*. *Curr Biol* *13*, 707-714.
- Lee, W.L., Kaiser, M.A., and Cooper, J.A. (2005). The offloading model for dynein function: differential function of motor subunits. *J Cell Biol* *168*, 201-207.
- Markus, S.M., and Lee, W.L. (2011a). Microtubule-dependent path to the cell cortex for cytoplasmic dynein in mitotic spindle orientation. *Bioarchitecture* *1*, 209-215.
- Markus, S.M., and Lee, W.L. (2011b). Regulated offloading of cytoplasmic dynein from microtubule plus ends to the cortex. *Dev Cell* *20*, 639-651.
- Markus, S.M., Punch, J.J., and Lee, W.L. (2009). Motor- and tail-dependent targeting of dynein to microtubule plus ends and the cell cortex. *Curr Biol* *19*, 196-205.
- McCarthy Campbell, E.K., Werts, A.D., and Goldstein, B. (2009). A cell cycle timer for asymmetric spindle positioning. *PLoS Biol* *7*, e1000088.
- McNally, F.J. (2013). Mechanisms of spindle positioning. *Journal of Cell Biology* *200*, 131-140.
- Moore, J.K., and Cooper, J.A. (2010). Coordinating mitosis with cell polarity: Molecular motors at the cell cortex. *Seminars in cell & developmental biology* *21*, 283-289.
- Moore, J.K., Li, J., and Cooper, J.A. (2008). Dynactin function in mitotic spindle positioning. *Traffic* *9*, 510-527.
- Morin, X., and Bellaiche, Y. (2011). Mitotic spindle orientation in asymmetric and symmetric cell divisions during animal development. *Dev Cell* *21*, 102-119.
- Nguyen-Ngoc, T., Afshar, K., and Gonczy, P. (2007). Coupling of cortical dynein and G alpha proteins mediates spindle positioning in *Caenorhabditis elegans*. *Nat Cell Biol* *9*, 1294-1302.
- Oegema, K., Desai, A., Rybina, S., Kirkham, M., and Hyman, A.A. (2001). Functional analysis of kinetochore assembly in *Caenorhabditis elegans*. *The Journal of Cell Biology* *153*, 1209-1226.
- Okumura, M., Natsume, T., Kanemaki, M.T., and Kiyomitsu, T. (2018). Dynein-Dynactin-NuMA clusters generate cortical spindle-pulling forces as a multi-arm ensemble. *eLife* *7*, e36559.
- Panbianco, C., Weinkove, D., Zanin, E., Jones, D., Divecha, N., Gotta, M., and Ahringer, J. (2008). A casein kinase 1 and PAR proteins regulate asymmetry of a PIP(2) synthesis enzyme for asymmetric spindle positioning. *Dev Cell* *15*, 198-208.

- Park, D.H., and Rose, L.S. (2008). Dynamic localization of LIN-5 and GPR-1/2 to cortical force generation domains during spindle positioning. *Dev Biol* 315, 42-54.
- Pecreux, J., Redemann, S., Alayan, Z., Mercat, B., Pastezeur, S., Garzon-Coral, C., Hyman, A.A., and Howard, J. (2016). The mitotic spindle in the one-cell *C. elegans* embryo is positioned with high precision and stability. *Biophys J* 111, 1773-1784.
- Pecreux, J., Roper, J.C., Kruse, K., Julicher, F., Hyman, A.A., Grill, S.W., and Howard, J. (2006a). Spindle oscillations during asymmetric cell division require a threshold number of active cortical force generators. *Curr Biol* 16, 2111-2122.
- Pecreux, J., Zimmer, C., and Olivo-Marin, J.C. (2006b). Biophysical active contours for cell tracking I: Tension and bending. In: *Ieee International Conference on Image Processing (Icip)*, October 8-11 2006, Atlanta, GA, USA, 1949-1952
- Pfister, K.K., and Lo, K.W.-H. (2012). Cytoplasmic Dynein Function Defined by Subunit Composition. In: *Dyneins : structure, biology and disease*, ed. S.M. King, Amsterdam ; Boston: Academic Press, 425-439.
- Preciado Lopez, M., Huber, F., Grigoriev, I., Steinmetz, M.O., Akhmanova, A., Koenderink, G.H., and Dogterom, M. (2014). Actin-microtubule coordination at growing microtubule ends. *Nat Commun* 5, 4778.
- Redemann, S., Baumgart, J., Lindow, N., Shelley, M., Nazockdast, E., Kratz, A., Prohaska, S., Bruges, J., Furthauer, S., and Muller-Reichert, T. (2017). *C. elegans* chromosomes connect to centrosomes by anchoring into the spindle network. *Nat Commun* 8, 15288.
- Redemann, S., Pecreux, J., Goehring, N.W., Khairy, K., Stelzer, E.H., Hyman, A.A., and Howard, J. (2010). Membrane invaginations reveal cortical sites that pull on mitotic spindles in one-cell *C. elegans* embryos. *PLoS One* 5, e12301.
- Redemann, S., Schloissnig, S., Ernst, S., Pozniakowsky, A., Ayloo, S., Hyman, A.A., and Bringmann, H. (2011). Codon adaptation-based control of protein expression in *C. elegans*. *Nat Methods* 8, 250-252.
- Riche, S., Zouak, M., Argoul, F., Arneodo, A., Pecreux, J., and Delattre, M. (2013). Evolutionary comparisons reveal a positional switch for spindle pole oscillations in *Caenorhabditis* embryos. *J Cell Biol* 201, 653-662.
- Roberts, A.J., Goodman, B.S., and Reck-Peterson, S.L. (2014). Reconstitution of dynein transport to the microtubule plus end by kinesin. *eLife* 3, e02641.
- Rose, L., and Gonczy, P. (2014). Polarity establishment, asymmetric division and segregation of fate determinants in early *C. elegans* embryos. *WormBook : the online review of C. elegans biology*, 1-43.
- Rostampour, A.R., Reeves, A.P., and Mitchell, O.R. (1988). Use of temporal variance for moving object extraction. *Computers and Communications*, 1988. Conference Proceedings., Seventh Annual International Phoenix Conference on, 480-484.
- Roul, J., Pecreux, J., and Tramier, M. (2015). Method for controlling a plurality of functional modules including a multi-wavelength imaging device, and corresponding control system. E.P. Office, WO2015144650 A1.
- Rousselet, J., Salome, L., Ajdari, A., and Prost, J. (1994). Directional motion of brownian particles induced by a periodic asymmetric potential. *Nature* 370, 446-448.

- Sage, D., Neumann, F.R., Hediger, F., Gasser, S.M., and Unser, M. (2005). Automatic tracking of individual fluorescence particles: application to the study of chromosome dynamics. *IEEE Transactions on Image Processing* *14*, 1372-1383.
- Sarov, M., Murray, J.I., Schanze, K., Pozniakovski, A., Niu, W., Angermann, K., Hasse, S., Rupprecht, M., Vinis, E., Tinney, M., Preston, E., Zinke, A., Enst, S., Teichgraber, T., Janette, J., Reis, K., Janosch, S., Schloissnig, S., Ejsmont, R.K., Slightam, C., Xu, X., Kim, S.K., Reinke, V., Stewart, A.F., Snyder, M., Waterston, R.H., and Hyman, A.A. (2012). A genome-scale resource for in vivo tag-based protein function exploration in *C. elegans*. *Cell* *150*, 855-866.
- Sarov, M., Schneider, S., Pozniakovski, A., Roguev, A., Ernst, S., Zhang, Y., Hyman, A.A., and Stewart, A.F. (2006). A recombineering pipeline for functional genomics applied to *Caenorhabditis elegans*. *Nat Methods* *3*, 839-844.
- Schmidt, D.J., Rose, D.J., Saxton, W.M., and Strome, S. (2005). Functional analysis of cytoplasmic dynein heavy chain in *Caenorhabditis elegans* with fast-acting temperature-sensitive mutations. *Mol Biol Cell* *16*, 1200-1212.
- Schmidt, R., Fielmich, L.E., Grigoriev, I., Katrukha, E.A., Akhmanova, A., and van den Heuvel, S. (2017). Two populations of cytoplasmic dynein contribute to spindle positioning in *C. elegans* embryos. *J Cell Biol* *216*, 2777-2793.
- Schonegg, S., Constantinescu, A.T., Hoegge, C., and Hyman, A.A. (2007). The Rho GTPase-activating proteins RGA-3 and RGA-4 are required to set the initial size of PAR domains in *Caenorhabditis elegans* one-cell embryos. *Proc Natl Acad Sci U S A* *104*, 14976-14981.
- Shaw, S.L., Yeh, E., Maddox, P., Salmon, E.D., and Bloom, K. (1997). Astral microtubule dynamics in yeast: a microtubule-based searching mechanism for spindle orientation and nuclear migration into the bud. *J Cell Biol* *139*, 985-994.
- Sheeman, B., Carvalho, P., Sagot, I., Geiser, J., Kho, D., Hoyt, M.A., and Pellman, D. (2003). Determinants of *S. cerevisiae* dynein localization and activation: implications for the mechanism of spindle positioning. *Curr Biol* *13*, 364-372.
- Sonnichsen, B., Koski, L.B., Walsh, A., Marschall, P., Neumann, B., Brehm, M., Alleaume, A.M., Artelt, J., Bettencourt, P., Cassin, E., Hewitson, M., Holz, C., Khan, M., Lazik, S., Martin, C., Nitzsche, B., Ruer, M., Stamford, J., Winzi, M., Heinkel, R., Roder, M., Finell, J., Hantsch, H., Jones, S.J., Jones, M., Piano, F., Gunsalus, K.C., Oegema, K., Gonczy, P., Coulson, A., Hyman, A.A., and Echeverri, C.J. (2005). Full-genome RNAi profiling of early embryogenesis in *Caenorhabditis elegans*. *Nature* *434*, 462-469.
- Splinter, D., Razafsky, D.S., Schlager, M.A., Serra-Marques, A., Grigoriev, I., Demmers, J., Keijzer, N., Jiang, K., Poser, I., Hyman, A.A., Hoogenraad, C.C., King, S.J., and Akhmanova, A. (2012). BICD2, dynactin, and LIS1 cooperate in regulating dynein recruitment to cellular structures. *Mol Biol Cell* *23*, 4226-4241.
- Srayko, M., Kaya, A., Stamford, J., and Hyman, A.A. (2005). Identification and characterization of factors required for microtubule growth and nucleation in the early *C. elegans* embryo. *Dev Cell* *9*, 223-236.
- Sugioka, K., Fielmich, L.E., Mizumoto, K., Bowerman, B., van den Heuvel, S., Kimura, A., and Sawa, H. (2018). Tumor suppressor APC is an attenuator of spindle-pulling forces during *C. elegans* asymmetric cell division. *Proc Natl Acad Sci U S A* *115*, E954-E963.

- Thery, M., Racine, V., Piel, M., Pepin, A., Dimitrov, A., Chen, Y., Sibarita, J.B., and Bornens, M. (2006). Anisotropy of cell adhesive microenvironment governs cell internal organization and orientation of polarity. *Proc Natl Acad Sci U S A* *103*, 19771-19776.
- van der Voet, M., Berends, C.W., Perreault, A., Nguyen-Ngoc, T., Gonczy, P., Vidal, M., Boxem, M., and van den Heuvel, S. (2009). NuMA-related LIN-5, ASPM-1, calmodulin and dynein promote meiotic spindle rotation independently of cortical LIN-5/GPR/Galpha. *Nat Cell Biol* *11*, 269-277.
- Widengren, J., Rigler, R., and Mets, U. (1994). Triplet-state monitoring by fluorescence correlation spectroscopy. *Journal of fluorescence* *4*, 255-258.
- Williams, S.E., Ratliff, L.A., Postiglione, M.P., Knoblich, J.A., and Fuchs, E. (2014). Par3-mInsc and Galphai3 cooperate to promote oriented epidermal cell divisions through LGN. *Nat Cell Biol* *16*, 758-769.
- Yoder, J.H., and Han, M. (2001). Cytoplasmic dynein light intermediate chain is required for discrete aspects of mitosis in *Caenorhabditis elegans*. *Mol Biol Cell* *12*, 2921-2933.
- Zheng, Z., Wan, Q., Liu, J., Zhu, H., Chu, X., and Du, Q. (2013). Evidence for dynein and astral microtubule-mediated cortical release and transport of Galphai/LGN/NuMA complex in mitotic cells. *Mol Biol Cell* *24*, 901-913.

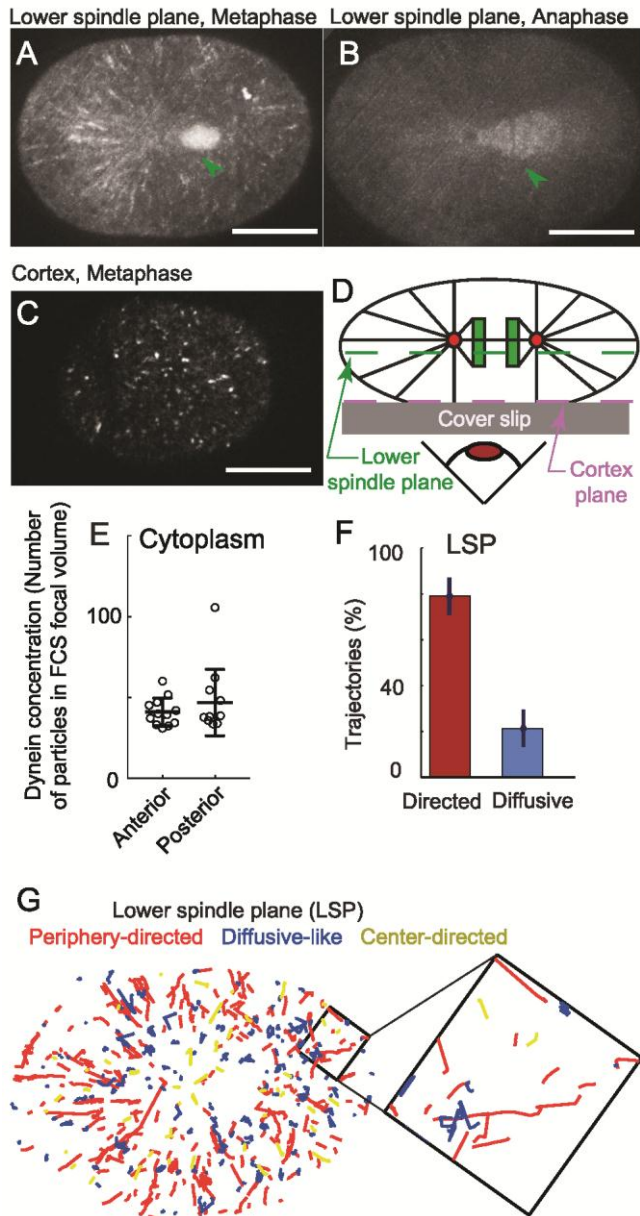


**Figure 1: Dynein intermediate chain DYCI-1::mCherry in the cytoplasm and at the cortex of *Caenorhabditis elegans*.**

Standard deviation map computed over 30 frames from a 5 frames/s DYCI-1::mCherry movie taken in the lower spindle plane (LSP) during (A) metaphase and (B) anaphase. (C) At the cell cortex during metaphase, DYCI-1::mCherry localized in a punctate manner. The mitotic spindle in the LSP is indicated by a green arrow. Scale bars, 10  $\mu$ m. (D) Schematic representation of the spinning disk confocal imaging setup depicting the spindle through its poles (red disks) from which emanate microtubules (black lines). The green rectangles are chromosomes and the dashed lines are the imaging planes at the LSP (green) and cortex (purple). (E) Dynein concentration in number of particles in the FCS focal volume (estimated at 0.3 fl) in the anterior and posterior embryo halves (Supplemental Text 1.3). Each circle corresponds to a single embryo. (F) Proportion of tracks in the LSP directed towards the cortex or diffusive-like averaged over  $N = 31$  embryos (8060 tracks). (G) Tracks detected in the LSP of a single embryo divided between those directed towards the cell periphery (red); towards the center (yellow); and those that display a diffusive-like motion, i.e. no clear direction (blue). Inset: zoom highlights the radial alignment of the directed tracks.

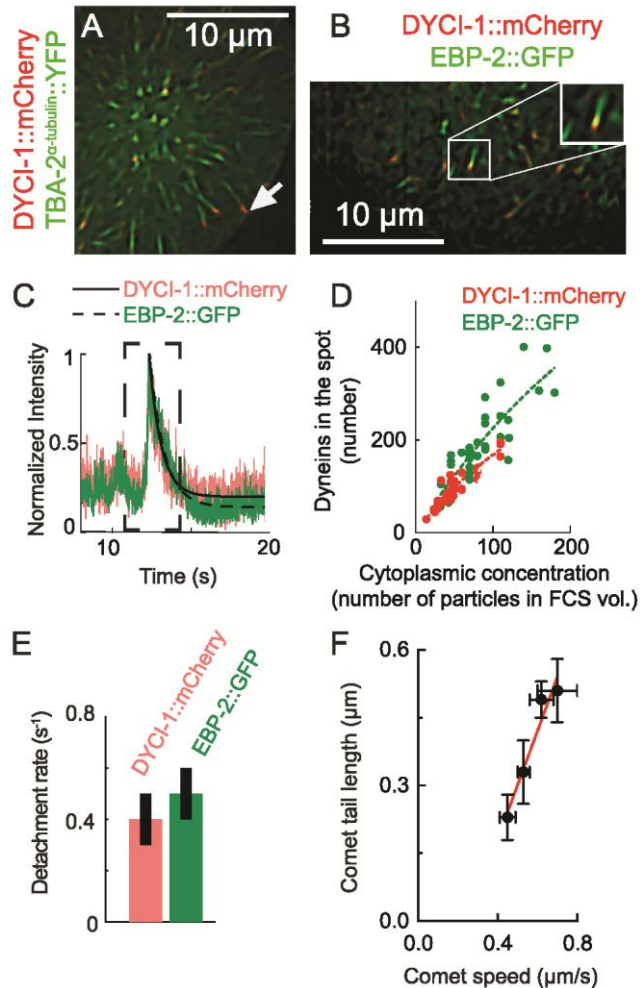


**Figure 2: DYCI-1::mCherry and EBP-2::GFP display similar dynamics at the microtubule plus-ends.**

(A) Micrograph displaying DYCI-1::mCherry (red) and TBA-2<sup>α-tubulin</sup>::YFP (green). The arrow indicates a microtubule plus end where DYCI-1::mCherry accumulates. (B) Micrograph of the metaphase of a *Caenorhabditis elegans* zygote, showing DYCI-1::mCherry (red) and EBP-2::GFP (green). These pictures come from the full sequence examples in Supplemental Figure S5A and C, respectively. (C) Intensity profile of a DYCI-1::mCherry and EBP-2::GFP spot crossing the focal volume during a fluorescence correlation spectroscopy experiment, normalized by the peak intensity. Thin black lines show the exponential fits for DYCI-1::mCherry (plain) and EBP-2::GFP (dashed), and the dashed outline indicates the concurrent peaks. (D) FCS measurements in DYCI-1::mCherry (red) and EBP-2::GFP (green) showing the number of dyneins (particles) in spots versus the dynein density in the cytoplasm (particles in the focal volume) (Supplemental Text 1.3-4). The dashed lines represent the fit of the experimental curves with an exponential growth ( $N = 8$  embryos, 43 spots) (Supplemental Text 4.1). (E) Detachment rates for doubly labelled DYCI-1::mCherry EBP-2::GFP embryos ( $N = 8$ ). These were obtained by fitting 43 individual FCS traces, as illustrated in (C). (F) Linear fit of DYCI-1::mCherry comet-tail lengths (30-50 profiles per condition) versus comet speed (typically 7 embryos and 1500 trajectories per condition) for various microtubule growth rates (Supplemental Text 4.2). The slope is  $1.2 \pm 0.2$  s, significantly different from zero ( $p = 0.03$ ). Error bars indicate the standard errors of the means.

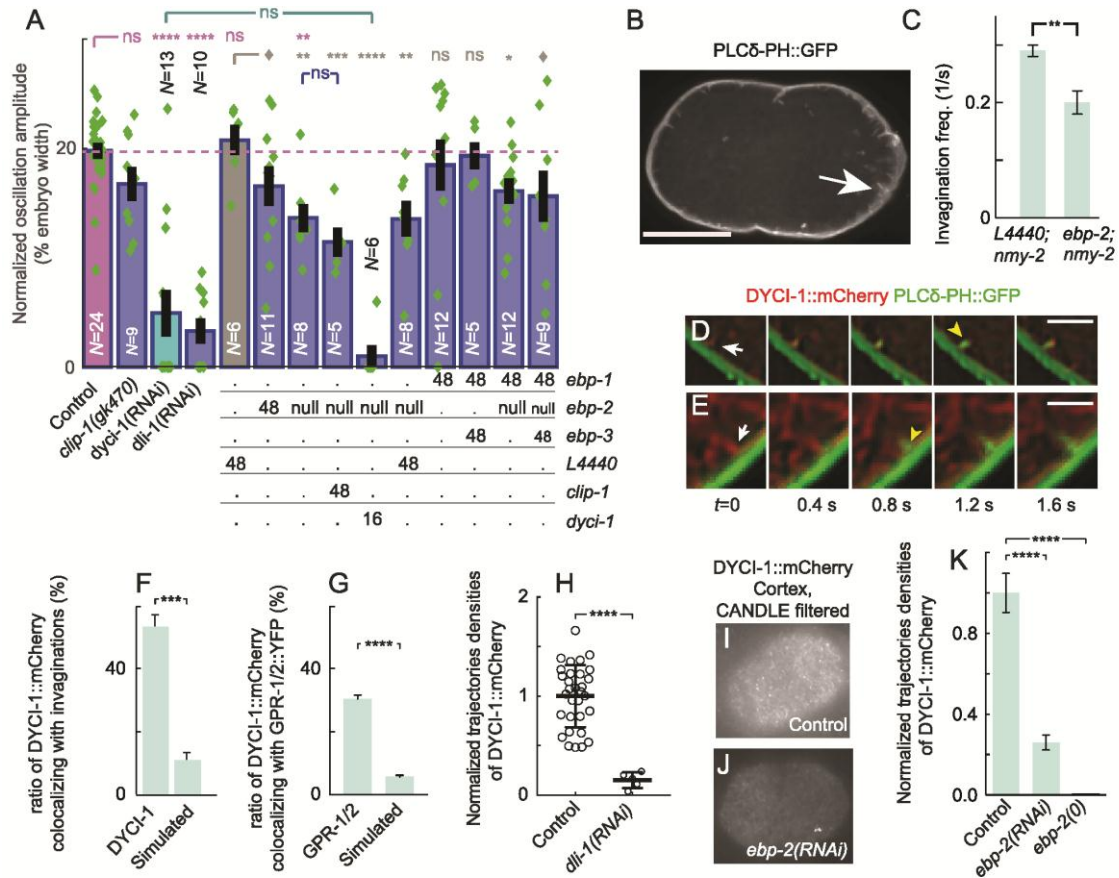


**Figure 3: Labeled dynein and its accumulation at the microtubule plus ends contributes to cortical forces.** (A) Maximum amplitudes of posterior centrosomal oscillations during anaphase as percentages of embryo width, upon various depletions of the EB homologs EBP-1/2/3, and with DYCI-1, DLI-1 and CLIP-1 partial depletions shown for reference. The table below the plot indicates various conditions: null for the *ebp-2(gk756)* null mutant; and 48 or 16 feeding hours for the RNAi experiments. Green diamonds correspond to raw data, and the horizontal pink dashed line indicates the amplitude for untreated embryos. Pink stars show the significance with respect to non-treated embryos, and grey ones with respect to control RNAi with the L4440 vector. Non-significant differences are indicated with “n.s.” in dark blue for *ebp-2(gk756)* with and without *clip-1(RNAi)*; and in light blue for *dyci-1(RNAi)* in the control and *ebp-2(gk756)* background. Centrosomes were labeled using the  $\gamma$ -tubulin::GFP construct. Error bars correspond to standard errors of the means. (B) Maximum intensity projection over 30 frames acquired at 2.5 frames/s for the doubly labeled strain with both DYCI-1::mCherry and PLC $\delta$ -PH::GFP, treated by *nmy-2(RNAi)* and viewed in the spindle plane. Scale bar, 10  $\mu$ m. The arrow indicates a good invagination example. (C) Invagination frequencies in double *nmy-2;ebp-2(RNAi)* ( $N = 6$ ) and its control *nmy-2;L4440(RNAi)* ( $N = 9$ ). Error bars indicate standard deviations, and the frequencies are significantly different. (D,E) Examples of invagination image sequences acquired during 15 frames at 2.5 frames/s in a doubly labeled strain upon *nmy-2(RNAi)*. Dynein and invaginations are viewed at the cell mid-plane. The PLC $\delta$ 1-PH::GFP channel is green, and DYCI-1::mCherry one is red. Dynein is seen arriving at the cortex then after a brief moment, it leaves along with an invagination. Membrane invaginations (yellow arrowheads) began after dynein appeared at the cortex (white arrows). Scale bars, 2  $\mu$ m. (F) Ratio of invaginations that colocalize with DYCI-1::mCherry tracks (left,  $N = 18$  embryos, 139 invaginations) and those that colocalize with an equal sample of simulated random trajectories. (G) Ratio of DYCI-1::mCherry tracks that colocalize with GPR-1/2::YFP ones in the doubly labeled strain (left,  $N = 8$  embryos, 3178 DYCI-1::mCherry tracks, and 6373 GPR-1/2::YFP ones) and those that colocalize with simulated random trajectories in an equal sample. Statistical significance was calculated using the Mann-Whitney/Wilcoxon test, and error bars indicate the standard errors of the means. (H) Trajectory densities at the cortex normalized by the mean in control embryos (Supplemental Text 2.4) for  $N = 31$  control and  $N = 5$  *dli-1(RNAi)* dynein light

intermediate chain subunit-treated embryos. Circles denote individual embryo values. Error bars indicate the standard errors of the means **(I)** Control and **(J)** *ebp-2(RNAi)*-treated DYCI-1::mCherry embryos imaged at the cortex after CANDLE pre-processing to enhance visibility (Supplemental Text 2.1). **(K)** Trajectory densities at the cell cortex and normalized against the DYCI-1::mCherry control ( $N = 6$ ) upon partial *ebp-2(RNAi)* ( $N = 9$ ) and after crossing with the *ebp-2(gk756)* null mutation ( $N = 3$ ). Differences are highly significant.

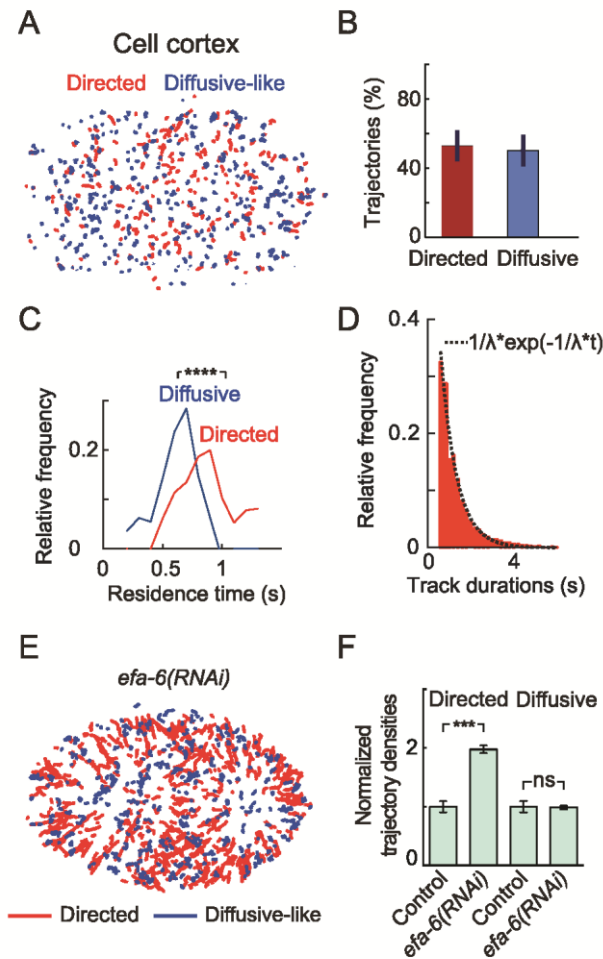


**Figure 4: Dynein dynamics at the cell cortex.**

(A) Directed (red) and diffusive-like tracks (blue) detected in a movie acquired at the cell cortex. (B) Proportion of directed and diffusive-like tracks at the cortex, averaged over  $N = 33$  embryos (9921 tracks). (C) Distributions of the residence time  $\lambda$  for directed and diffusive-like tracks at the cell cortex ( $N = 26$  embryos, 9595 tracks). Stars indicate a significant difference between the corresponding mean values. (D) Histogram example of the durations at the cell cortex for the diffusive-like tracks of a typical embryo fitted to an exponential with a residence time  $\lambda$  of 0.7 s. (E) Tracks detected at the cell cortex in an *efa-6(RNAi)*-treated embryo, with the same representation as in (A). (F) Normalized track densities at the cell cortex in  $N = 7$  control embryos (3000 tracks) and in  $N = 9$  embryos (1400 tracks) treated with *efa-6(RNAi)*.

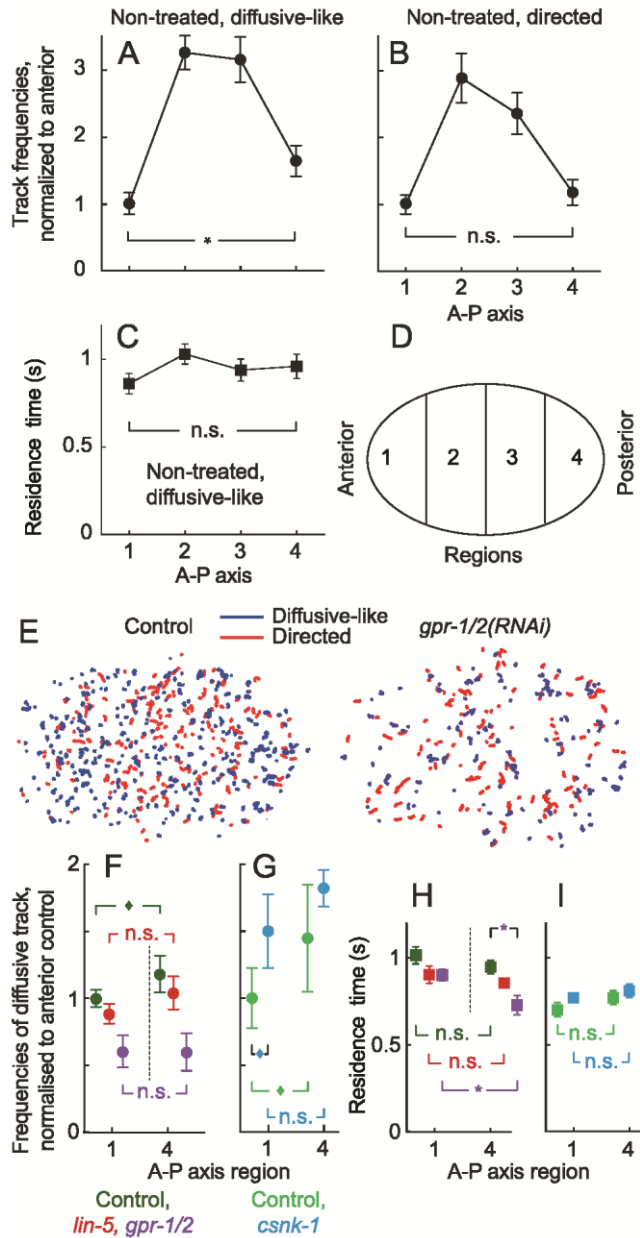


**Figure 5: GPR-1/2 regulate DYCI-1::mCherry dynamics at the cell cortex.**

(A) Diffusive-like and (B) directed track frequencies, the number of tracks at the cell cortex per unit of time (Supplemental Text 2.4) normalized by the value in the anterior-most region (D, region 1). These were analyzed along the AP axis within four regions having equal lengths (see panel d) in  $N = 7$  non-treated DYCI-1::mCherry embryos. Using the paired  $t$ -test, we compared the values between the external regions, which are the only relevant ones to force imbalance (see main text), and found a significant difference. (C) Residence times for the tracks plotted in (A). (D) Schematic of the four regions used to analyze the tracks. (E) Directed (red) and diffusive-like tracks (blue) detected at the cell cortex in control (left) and *gpr-1/2(RNAi)*-treated embryos (right). (F,G) Frequencies of diffusive-like tracks normalized by the value from the anterior-most region of the control (circles). Embryos shown are (F) treated with *gpr-1/2(RNAi)* (purple,  $N = 4$ ) or *lin-5(RNAi)* (red,  $N = 5$ ); control (dark green,  $N = 3$ ); and (G) treated with *csnk-1(RNAi)* (light blue,  $N = 9$ ) and corresponding control (light green,  $N = 5$ ). (H,I) Residence times at the cell cortex (squares) of the same treated and control embryos as shown in (F,G), also analyzed only in the anterior- and posterior-most regions. Error bars indicate the standard errors of the means. Brackets indicate statistical significances, either comparing anterior/posterior in the same condition, or treatment against the corresponding control in the same area. For clarity's sake, most non-significant indications were omitted.

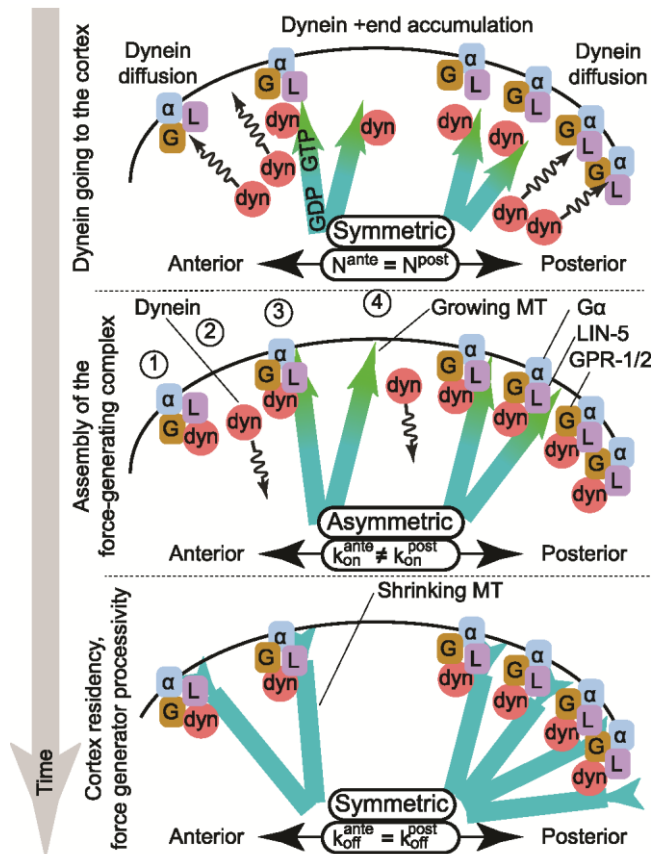


**Figure 6: Dynein arrival and residence at the cortex highlights the possible causes of force imbalance.**

Schematic views of the arrival, attachment, and residence of dynein at the cell cortex. (**Top**) Dynein (red “dyn” disks) arrive at the cortex in equal quantities from the posterior and anterior embryo halves, either by 3D diffusion (squiggly arrows) or after indirect hitchhiking on EBP-2 and accumulation at the plus ends of growing microtubules (blue/green GTP-capped arrows). Other members of the trimeric complex, GPR-1/2 (orange “G” blobs) and LIN-5 (purple “L” blobs), are anchored at the cortex by  $\text{Ga}$  GPA-16 and GOA-1 (blue “ $\alpha$ ” blobs). The total amounts of dynein available at the anterior and posterior sides of the cortex are equal. (**Middle**) GPR-1/2 (and other complex members) are enriched on the posterior side. They bind the dynein that arrives by 3D diffusion (1) or via plus-end accumulation (3). Dyneins that do not find a cortical anchor (GPR-1/2 complex) leave the cortex (2,4). The attachment rate is therefore higher on the posterior side, which leads to more active force generators there. (**Bottom**) Bound dyneins pull on astral microtubules that concurrently depolymerize (blue bars). The symmetrical unbinding rate leads to equal residence times in the posterior and anterior regions.

Table 1 lists the primers used for amplification.

Target	Forward primer	Reverse primer
<i>ebp-1/3</i>	5' ACCGGGAGTCGATATGGC 3'	5' TCAACATTTCCAATCGATTCAAT 3'
<i>ebp-1</i>	5' TCGTCTTGAATTGGATTGGC TTTCCAACCTGGAAACTAGTGCA GACTACGTGGAAGAATTT 3' 5' GATTAAGGGAAAAATTCAGG ACAACCTTGAATTCTTGCAATG GTTCAAGAAATTTGTTTCGATGCT AACTATGATGGACATGAGTAT GA 3'	5' TTGTCCTGAAATTTCCCTTAATC AATTTATCAACAGGAATCACTTTCT CGACACCCAAATTTCTTCCACGTAGT CTGCAC 3' 5' CATTACGTGCTTGCATTGGATCA TACTCATGTCCATCATAGTTAGC 3'